Double quantum well segments in ballistic diode bases

Z. S. Gribnikov,[a] A. N. Korshak,[b] and V. V. Mitin
Department of Electrical and Computer Engineering, Wayne State University, Detroit, Michigan 48202

(Received 7 July 1997; accepted for publication 18 October 1997)

We consider space charge limited ballistic electron transport in short current-conducting channels formed by single and double quantum well segments. Independent contacts to the bottom-well and the top-well forming the double quantum well segment is stipulated. Three different structures are simulated: a resonant overlap structure, a resonant cover structure, and a coupler structure. It is shown that anode currents in these structures oscillate with increasing voltage across the structure, resulting in repeatedly N-shaped current–voltage ($I-V$) characteristics. A modulation level of the current oscillations is close to 100%. The shape of these oscillations is substantially asymmetric both for the overlap and the cover structures. The asymmetry is due to a very strong nonlinear space charge modulation, and N-shaped parts of $I-V$ characteristics can become Z-shaped when a strong tunnel connection in the double quantum well segment takes place. In the coupler structure the modulation of partial anode currents flowing out through each of two anodes, which are independently contacted to the bottom-well and the top-well, occurs only. The space charge increases monotonously with the voltage. Justification criteria of the classic approach used in our calculations are discussed in detail. © *1998 American Institute of Physics.*
[S0021-8979(98)00603-3]

I. INTRODUCTION

Lately experimental investigation of electron phenomena in a double quantum well (DQW) with independent electric contacts to the quantum wells (QWs) forming the DQW have been developed owing to efforts of several groups. They have suggested[1–8] a set of different technological methods for independent contacting to the individual wells of the DQW that are separated by a narrow tunnel barrier. Such independently contacted DQW structures have been applied for the experimental study of a field-induced resonant tunneling between two parallel two-dimensional electron gases (2DEGs),[9,10] magnetotunneling,[1,11–13] compressibility of 2DEGs and 2D hole gases,[14,15] probing the Fermi-surfaces of 2DEGs by tunneling,[16] etc. All these and a number of other works have dealt with the long DQW segments ($\sim$100 μm) and dissipative (diffusive) electron (or hole) transport in the wells.

On the other hand, there exists another interesting subject dealing with double quantum waveguides. It is an electron directional coupler.[17,18] Usually a segment of a double quantum wire is used in the coupler design (see Refs. 19 and 20 and references therein), but there are several design suggestions based on DQW structures.[21–25] A substantial difference between the electron directional coupler and the structures realized in Refs. 1–16 is that the former is a ballistic device and electrons have to pass it without scattering. A problem of the formation of the short double wire segment with independent contacts to the wires is solved on the whole by using the split-gate architecture[19] or by ion-beam scanning.[20] At the same time we know nothing about successful experimental implementation of short ballistic DQW segments (DQWSs) and we have to refer to the methods suggested in Refs. 1–8 (with further progress in shortening of the longitudinal size of shallow ohmic contacts, front and back gates, and other elements of contacting, controlling, and isolation).

Here we examine nonlinear space charge limited longitudinal ballistic electron transport in a short DQWS. It is the first consideration of the presented problem. Three different contacting schemes with the wells forming the DQW are considered (Fig. 1). The cathode is always contacted to the bottom-well and the dissimilarity between the schemes consists of different position of the anode contacts.

For a resonant overlap structure (ROS) [Fig. 1(a)] the anode contacts to the top-well. This design is similar to the design of the structures used in Refs. 3, 4, 9, 10, 12, and 16, which are manufactured for other then our goals. In a resonant cover structure (RCS) [Fig. 1(b)] both electrodes are contacted to the bottom-well. The DQWS is separated from the cathode and the anode by single quantum well segments (SQWSs). A need of the left (cathode-adjacent) SQWS with a length l_1 will be substantiated later. The right (anode-adjacent) SQWS is not obligatory but it might happen to be unavoidable in the real experimental design. A linear ballistic conductance of the ROS and the RCS was considered in Refs. 23, 26, and 27. Such a linear problem does not require to take into account a self-consistent space charge problem and electron acceleration due to the anode voltage, which are the basic for the considered here nonlinear problem. Figure 1(c) shows a coupler structure. It is a version of the electron directional coupler considered preliminarily in Ref. 28. This structure has two anodes, and therefore, we have two anode currents.

A main distinctive feature of this article is a consideration of the nonlinear ballistic regime with a charge limitation of the electron current. This means that a ballistic transport problem is solved self-consistently with a problem of a potential distribution in the current-conducting channel and

[a]On leave from the Institute of Semiconductor Physics, Kiev 252028, Ukraine.
[b]Also on leave from the Institute of Semiconductor Physics, Kiev 252028, Ukraine; electronic mail:zinovi@besm6.eng.wayne.edu

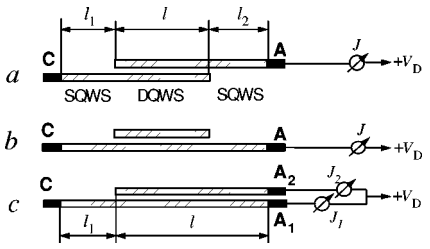

FIG. 1. Three types of considered structures with the DQWSs: (a) the resonant overlap structure; (b) the resonant cover structure; (c) the coupler structure with two anodes.

everywhere around it (as in Refs. 29 and 30 for analogous problems). This regime is particularly interesting for two reasons.

First of all, a momentum distribution of the ballistic electrons in the DQWS differs from the Fermi-distribution, becoming outstretched along a current direction. A transport regime is approaching a single-velocity regime, that is the electron beam consists of the electrons of approximately the same velocity. Therefore the path $L(\tau)$, which electrons pass during a time $\tau=h/2\delta\epsilon$ is also the same [where $2\delta\epsilon$ is a value of the symmetric–antisymmetric (SAS) splitting in the DQW, $2\delta\epsilon=\epsilon_2-\epsilon_1>0$, and $\epsilon_{1,2}$ are energies of the two lowest subbands in the DQW]. For a weak tunnel coupling we have: $\delta\epsilon\ll\epsilon_{1,2}$. In this manner all the electrons entered in the bottom-well of the DQWS transfer into the top-well at the moment $t=\tau/2$ of their movement in the DQWS passing distance $L(\tau/2)$ from the left boundary of the segment. They return to the bottom-well at $t=\tau$, passing distance $L(\tau)$ etc. In this sense the 2DEG under consideration reminds us of the 1DEG because there is no transverse velocity and the picture of interwell transitions in the DQWS is similar to the picture of interwire transitions in the double quantum wire segment.

The number of the interwell transitions during one passing over the DQWS depends on a mean electron velocity, v_{DQW}. The velocity is conditioned by the applied voltage, V_D, which accelerates the electrons. In this manner, V_D determines whether the electrons are reflected from the well deadlock (in the bottom-well for the ROS and in the top-well for the RCS). Therefore, the ballistic current in these structures oscillates repeatedly as a function of the applied voltage V_D, i.e., the $I-V$ characteristics consist of several N-shaped regions.

Second, the electron reflection from the well deadlocks in the DQWS forces a part of electrons entered into the base from the cathode to come back (the base is a region between heavily doped anode and cathode). In addition, an electron charge accumulates in the DQWS if it is an electron cavity (as it takes place in the ROS and the RCS). These effects lead to an increase in the space electron charge in the base of the diode and promote space charge limitation of the current. Therefore, a current modulation by V_D can be very strong and Z-shape of the JV_D-characteristics with a hysteresis can appear, as a result.

For the coupler structure there is no substantial electron reflection if the anode contacts A_1 and A_2 [Fig. 1(c)] are assumed to be nonreflecting. So the total current, $J=J_1+J_2$, does not oscillate as a function of V_D in contrast to the partial currents J_1 and J_2, flowing through the anodes A_1 and A_2, respectively. The partial currents vary from 0 to J in counterphase.

For completing cumbersome numerical calculations we undertake the following simplified assumptions: (i) The DQW is assumed symmetrical and conditions of the tunnel resonance are satisfied precisely everywhere in the DQWS. (ii) Charge asymmetry (i.e., asymmetry induced by electron transfer from one well to the other) is assumed to be small. It does not lead to substantial tunnel resonance detuning. Since a stationary interwell redistribution of electrons is the cornerstone of all the considered effects, conditions of the applicability of this assumption will be discussed further in the proper place. (iii) There are two different types of current oscillations versus voltage. The current oscillations of the first type (CO-1) appear due to the interwell tunnel transfer in the DQWS with the characteristic length $L(\tau)=\tau v_{\mathrm{DQW}}$. The current oscillations of the second type (CO-2) appear due to the electron wave reflections from the well deadlocks in the ROS and the RCS. The DQWSs in these structures are electron wave cavities, and their modes are determined by a correlation of length l and mean electron wave length λ_{DQW}. These oscillations would manifest themselves simultaneously in the single-velocity regime of the transport in the DQWS. But broadening of the velocity distribution in the real ballistic beams and inhomogeneities of the segment length lead to suppression of the CO-2. The similar effects for the case of the linear ballistic conductance were considered thoroughly in Ref. 26. Taking into account the suppression of the CO-2, the electrons can be considered as classical particles ($\lambda_{\mathrm{DQW}}=0$), which may tunnel between the QWs despite all. Criterion of this approach is based on a strong inequality:

$$\tau v_{\mathrm{DQW}}\gg\lambda_{\mathrm{DQW}}. \tag{1}$$

This condition can be led down to $eV_D\gg\delta\epsilon$ and allows us to choose such intervals of V_D and energy width of the ballistic electron beam μ^* that the CO-2 (with a small voltage period) are suppressed while the CO-1 (with a large voltage period) are displayed clearly. It should be mentioned that there are no CO-2 in the coupler structure because there is no electron resonant cavity here and both the cathode and the anodes are assumed to be absorbing, i.e., nonreflecting.

The stable and repeated N-shaped and Z-shaped JV_D-characteristics in the ROS and the RCS can be used for generation and amplification of subterahertz and terahertz electric oscillations and for high-speed electron switches.

The structure of this article is as follows: A general consideration of the problem will be given in Sec. II. Results of numerical calculations for the ROS and the RCS are described in Sec. III, and results for the couplers are presented in Sec. IV. The discussion and summary are given in Secs. V and VI, respectively.

II. GENERAL CONSIDERATION

A ballistic electron distribution function $F(\mathbf{k},x)$ conserves along the characteristics:

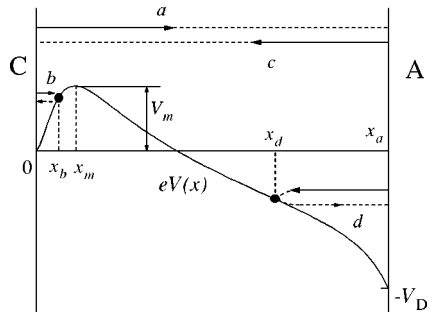

FIG. 2. Distribution of the potential energy $-|e|V(x)$ and possible electron paths.

$$\frac{\hbar^2 k_x^2}{2m} - |e|V(x) = \epsilon_x = \text{const}, \tag{2}$$

$$k_y = \text{const}, \tag{3}$$

where $\mathbf{k}=(k_x,k_y)$ is the in-plane wave vector and the axis x is in the current direction, $V(x)$ is the electrostatic potential in the current-conducting channel, m is the longitudinal effective mass. This means that

$$F(\mathbf{k},x) = f^{(\pm)}(\epsilon_x,k_y). \tag{4}$$

We use designations $f^{(+)}(\epsilon_x,k_y)$ for $k_x>0$ and $f^{(-)}(\epsilon_x,k_y)$ for $k_x<0$.

The stationary potential energy $eV(x)=-|e|V(x)$ for the ordinary ballistic diodes has a single maximum at $x=x_m$, $V_m=-V(x_m)$ (Fig. 2) in the space charge limited transport regime, or this energy is monotonous in the current saturation regime (more details on the potential distribution can be found in Ref. 29). When $eV(x)$ has at least one minimum, a ballistic problem is not determined completely and it requires additional equations. The single maximum is called the effective cathode and we can consider four groups of ballistic electrons (Fig. 2): Group (a): Cathode electrons (entered into the base from the cathode) with $\epsilon_x>|e|V_m$ that reach the anode. For these electrons we have

$$\begin{aligned} &k_x = |k_x| = \sqrt{2m(\epsilon_x+|e|V(x)}/\hbar > 0, \\ &f^{(+)}(\epsilon_x,k_y) = F_0(\epsilon-\mu), \end{aligned} \tag{5}$$

where $F_0(\epsilon-\mu)$ is a Fermi–Dirac distribution with Fermi-energy μ, $\epsilon=\epsilon_x+\hbar^2k_y^2/2m$. Group (b): Cathode electrons with $\epsilon_x<|e|V_m$ that come back to the cathode after reflection at x_b:

$$\begin{aligned} &k_x = \pm|k_x|, \\ &f^{(+)}(\epsilon_x,k_y) = f^{(-)}(\epsilon_x,k_y) = F_0(\epsilon-\mu), \quad 0<x<x_b<x_m, \end{aligned} \tag{6}$$

where the signs ''+'' and ''−'' refer to the electrons before and after the reflection. Group (c): Anode electrons with $\epsilon_x>|e|V_m$ that reach the cathode:

$$\begin{aligned} &k_x = -|k_x|, \\ &f^{(-)}(\epsilon_x,k_y) = F_0(\epsilon-\mu-|e|V_D). \end{aligned} \tag{7}$$

Here μ is a Fermi-energy for the anode electrons which is assumed to be equal to the Fermi-energy for the cathode electrons. The zero of the electron energy is the same for the cathode and the anode electrons. Group (d): Anode electrons with $\epsilon_x<|e|V_m$ that come back to the anode after reflection at x_d:

$$\begin{aligned} &k_x = \mp|k_x|, \\ &f^{(-)}(\epsilon_x,k_y) = f^{(+)}(\epsilon_x,k_y) = F_0(\epsilon-\mu-|e|V_D), \\ &x_m<x_d<x<x_a. \end{aligned} \tag{8}$$

The signs ''−'' and ''+'' refer to the electrons before and after the reflection, respectively, and x_a is a coordinate of the anode.

If the DQWS is embedded into the ballistic diode base, we have to take into consideration additional components of the distribution function. We introduce functions $f_b^{(\pm)}(\epsilon_x,k_y,x)$ and $f_t^{(\pm)}(\epsilon_x,k_y,x)$ where the subscripts b and t indicate belonging to the bottom- and top-wells:

$$f_{t,b}^{(\pm)}(\epsilon_x,k_y,x) = \nu_{t,b}^{(\pm)}(x) f^{(\pm)}(\epsilon_x,k_y), \tag{9}$$

with $\nu_{t,b}^{(\pm)}(x)$ obeying the following conditions:

$$0 \leqslant \nu_{t,b}^{(\pm)} \leqslant 1, \quad \nu_t^{(\pm)} + \nu_b^{(\pm)} = 1. \tag{10}$$

To solve the considered nonlinear transport problem we should determine $\nu_{t,b}^{(\pm)}(x)$ and $f^{(\pm)}(\epsilon_x,k_y)$ everywhere in the ballistic diode base for an arbitrary potential distribution $V(x)$.

An interwell electron redistribution is determined by the interference of two pairs of electron waves expanding in the DQWS. These pairs relate to SAS-splitting subbands with the energies ϵ_1 and ϵ_2. The pairs of waves have slightly different values of $\epsilon_{x1,2}$, $\epsilon_{x1,2}=\epsilon_x\pm\delta\epsilon$, and $|k_{x1,2}|$, $|k_{x1,2}| = \sqrt{2m[\epsilon_{x1,2}+|e|V(x)]}/\hbar$. A phase difference which determines interwell electron redistribution in the DQWS is equal to

$$\varphi^{(\pm)}(\epsilon_x,x) = \int_{x_o^{(\pm)}}^{x} \delta k(\epsilon_x,x')\,dx', \tag{11}$$

where

$$\delta k(\epsilon_x,x) = (|k_{x1}|-|k_{x2}|)/2 \simeq \frac{m}{\hbar}\cdot\frac{\delta\epsilon}{\sqrt{2m[(\epsilon_x+|e|V(x))]}}, \tag{12}$$

and $x_o^{(\pm)}$ are determined from the boundary conditions and differ for different directions of wave propagation. Equation (12) is written for $\delta\epsilon \ll \epsilon_x$. According to Refs. 23 and 28 phase coefficients $\nu_{t,b}^{(\pm)}$ are selected in the form:

$$\nu_b^{(\pm)} = \cos^2\,\varphi^{(\pm)}(\epsilon_x,x), \quad \nu_t^{(\pm)} = \sin^2\,\varphi^{(\pm)}(\epsilon_x,x). \tag{13}$$

To determine $x_o^{(\pm)}$ and $\nu_{t,b}^{(\pm)}$ we use the following boundary conditions. At the nonreflecting (open) boundaries we specify the distribution functions of the electrons entering into the DQWS: $f_{t,b}^{(+)}(\epsilon_x,k_y,0)$ and $f_{t,b}^{(-)}(\epsilon_x,k_y,l)$, while at the reflecting boundaries (the well deadlocks) we use equations:

$$\begin{aligned} &f_{t,b}^{(+)}(\epsilon_x,k_y,0) = f_{t,b}^{(-)}(\epsilon_x,k_y,0), \\ &f_{t,b}^{(+)}(\epsilon_x,k_y,l) = f_{t,b}^{(-)}(\epsilon_x,k_y,l). \end{aligned} \tag{14}$$

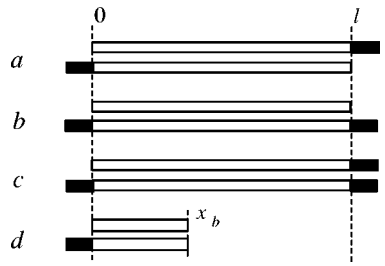

FIG. 3. The DQW segments of the structures represented in Fig. 1; cases (a), (b), and (c) correspond to (a), (b), and (c) in Fig. 1, respectively; (d) is a case of the potential reflection at the point $x=x_b$.

The DQWSs for the structures in Figs. 1(a)–1(c) are presented in Figs. 3(a)–3(c), respectively (with a new position of the origin of the x-axis). The nonreflecting boundaries are furnished with tips while the reflecting deadlocks have no tips.

At first we consider in detail the case shown in Fig. 3(c) with $f_b^{(+)}(\epsilon_x,k_y,0)=f(\epsilon_x,k_y)\equiv f$ and $f_{t,b}^{(-)}(\epsilon_x,k_y,l)=0$. In this case, we have $f_{t,b}^{(-)}(\epsilon_x,k_y,x)=0$ everywhere. This means that $f_t^{(+)}(\epsilon_x,k_y,0)=0$, $x_o^{(+)}=0$, $\varphi^{(+)}(\epsilon_x,x)=\int_0^x \delta k(\epsilon_x,x')dx'\equiv\xi(x)$, and

$$f_b^{(+)}(\epsilon_x,k_y,x)=f\cdot\cos^2\ \xi(x),$$
$$f_t^{(+)}(\epsilon_x,k_y,x)=f\cdot\sin^2\ \xi(x). \tag{15}$$

We designate the coefficients of transmission to the bottom-anode and to the top-anode as t_b and t_t:

$$t_b\equiv t_b(\epsilon_x)=\cos^2\ \xi(l),\quad t_t\equiv t_t(\epsilon_x)=\sin^2\ \xi(l)=1-t_b. \tag{16}$$

These coefficients oscillate with a variation of the phase $\xi(l)$. In the linear directional couplers we have to vary either the tunnel coupling of the wells (i.e., $\delta\epsilon$) or the Fermi-energy of the electrons entering into the DQWS with the help of a special gate. But in a considering nonlinear situation variations of the voltage V_D and consequently the potential distribution $V(x)$ lead to oscillations of t_b and t_t.

Now we consider the coupler–structure for the reverse direction of the current. If $f_b^{(-)}(\epsilon_x,k_y,l)=f_1(\epsilon_x,k_y)\equiv f_1$ and $f_b^{(+)}(\epsilon_x,k_y,0)=f_t^{(-)}(\epsilon_x,k_y,l)=0$, we obtain

$$f_b^{(-)}(\epsilon_x,k_y,x)=f_1\cos^2\ \xi'(x),$$
$$f_t^{(-)}(\epsilon_x,k_y,x)=f_1\sin^2\ \xi'(x), \tag{17}$$

where $\xi'(x)=\xi(l)-\xi(x)$. After the reflection from the top-well deadlock at $x=0$ we have

$$f_t^{(+)}(\epsilon_x,k_y,x)=f_1t_t\cos^2\ \xi(x),$$
$$f_b^{(+)}(\epsilon_x,k_y,x)=f_1t_t\sin^2\ \xi(x). \tag{18}$$

The coefficient of transmission in the reverse direction is equal to $T^{(r)}=t_b$ and the coefficients of reflection into the bottom- and top-wells are $R_b^{(r)}=t_t^2$, $R_t^{(r)}=t_bt_t$.

Due to the symmetry of the anodes we have to assume $f_t^{(-)}(\epsilon_x,k_y,l)=f_b^{(-)}(\epsilon_x,k_y,l)=f_1$. This leads to $f_t^{(+)}=f_1\cos^2\xi(x)$, $f_b^{(+)}=f_1\sin^2\xi(x)$ and, as a result, we have $R_b^{(r)}=t_t/2$, $R_t^{(r)}=t_b/2$ and $T^{(r)}\equiv 1/2$.

Now we turn to the ROS [Fig. 3(a)]. For $f_b^{(+)}(\epsilon_x,k_y,0)=f$, $f_t^{(-)}(\epsilon_x,k_y,0)=0$ we obtain

$$f_b^{(+)}(\epsilon_x,k_y,x)=f\cos^2\ \xi(x)+f_1\sin^2\ \xi(x),$$
$$f_t^{(+)}(\epsilon_x,k_y,x)=f\sin^2\ \xi(x)+f_1\cos^2\ \xi(x), \tag{19}$$

$$f_b^{(-)}(\epsilon_x,k_y,x)=f_2\cos^2\ \xi'(x),$$
$$f_t^{(-)}(\epsilon_x,k_y,x)=f_2\sin^2\ \xi'(x), \tag{20}$$

where functions $f_1=f_1(\epsilon_x,k_y)$ and $f_2=f_2(\epsilon_x,k_y)$ are determined by the boundary conditions (14):

$$f_1=f_t^{(+)}(\epsilon_x,k_y,0)=\frac{ft_t}{1+t_t},$$
$$f_2=f_b^{(-)}(\epsilon_x,k_y,l)=\frac{f}{1+t_t}. \tag{21}$$

The transmission and reflection coefficients are equal to

$$T=t_t+t_bf_1/f=2t_t/(1+t_t), \tag{22}$$

$$R=t_bf_2/f=t_b/(1+t_t)=1-T. \tag{23}$$

For the RCS [Fig. 3(b)] instead of Eq. (20) we obtain

$$f_b^{(-)}(\epsilon_x,k_y,x)=f_2\sin^2\ \xi'(x),$$
$$f_t^{(-)}(\epsilon_x,k_y,x)=f_2\cos^2\ \xi'(x). \tag{24}$$

Functions f_1 in Eq. (19) and f_2 in Eq. (24) according to the boundary conditions (14) for the RCS are equal to

$$f_1=f_t^{(+)}(\epsilon_x,k_y,0)=\frac{ft_b}{1+t_b},$$
$$f_2=f_t^{(-)}(\epsilon_x,k_y,l)=\frac{f}{1+t_b}, \tag{25}$$

$$T=2t_b/(1+t_b),\quad R=t_t/(1+t_b)=1-T. \tag{26}$$

Figure 3(d) relates to the situation when the cathode electrons are reflected from the potential barrier at x_b in the DQWS, if $0<x_b<l$, and to the analogous case for the anode electrons. Naturally there is no interwell redistribution and

$$f_b^{(\pm)}(\epsilon_x,k_y,x)=f_t^{(\pm)}(\epsilon_x,k_y,x)=f(\epsilon_x,k_y). \tag{27}$$

It should be mentioned that a sheet concentration ratio at the SQWS/DQWS boundary, $(x=0)$, is

$$\zeta=\frac{f_b^{(+)}+f_b^{(-)}+f_t^{(+)}+f_t^{(-)}}{f_b^{(+)}+f_b^{(-)}}=2, \tag{28}$$

i.e., there is a concentration discontinuity at the boundary. This is because the density of states in a DQW twice exceeds the density of states in a single well. Under these conditions, a real ballistic equilibrium takes place.

The ratio ζ at $x=0$ is:

$$\zeta=1+t_t \tag{29}$$

for the ROS and

$$\zeta=1+t_b \tag{30}$$

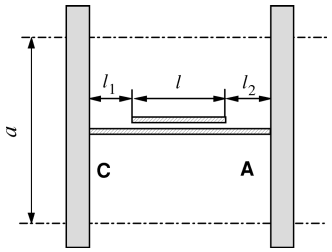

FIG. 4. The model element of the spatial periodic structure.

for the RCS. This ratio is equal to 2 under the conditions of full transmission, $t_{b,t}=1$ (no reflection!). When $t_{b,t}=0$ (full reflection) we obtain $\zeta=1$ and there is no sheet concentration jump at the boundary.

The above obtained formulas cannot be applied directly till the self-consistent potential distribution $V(x)$ inside and outside the DQWS is known. Therefore we incorporate the DQWS block in the full self-consistent procedure of the calculations. The equilibrium Fermi-distribution of the electrons entering from the n^+-contacts specifies the functions $f^{(\pm)}(\epsilon_x,k_y,x)$ for the electrons in the base. The geometry of the diode defines the self-consistent potential $V(x)$ in a current-conducting channel. In addition to the 2DEG parameters (the effective mass, m, the SAS-energy splitting, $2\delta\epsilon$, and the Fermi-energy, μ), the ballistic current problem is described by parameters of the ballistic structure and the geometry of the surroundings. They are the donor concentration in the base, N_b [cm^{-2}], the lengths of the cathode-adjacent SQWS, l_1, the anode-adjacent SQWS, l_2, and the DQWS, l. Here we consider a flat capacitor with equipotential plates $C(V=O)$ and $A(V=V_D)$ (Fig. 4) and a dielectric constant ϵ_d. The plates are connected by current-conducting channels which are the diode bases and which form a spatial periodic system with a period a. The base channel can be considered as almost a solitary when $a>l+l_1+l_2$, and results are independent of a (or depend slightly, see, for details Ref. 29). The self-consistent problem with a one-dimensional ballistic kinetic equation and a 2D Poisson-equation is solved numerically.

III. RESULTS FOR RESONANT OVERLAP AND COVER STRUCTURES

Before the results of our calculations are presented, we will sketch the JV_D-dependences of the ROS and the RCS qualitatively. The current has to reach its maximum values when $t_{t,b}=1$. If there are no redistribution of the self-consistent potential $V(x)$, these conditions have a form:

$$2\int_0^l \delta k(\epsilon_x,x)dx=\pi(2s+1/2\pm 1/2),\quad s=0,1,2,\ldots, \tag{31}$$

where ''+'' relates to the ROS, and ''−'' relates to the RCS. In the single-velocity approximation $\epsilon_x\simeq|e|V_m$, and we have [see Eq. (12)]

$$\delta k(\epsilon_x,x)\simeq\delta k(x)\simeq\frac{m\delta\epsilon}{\hbar[2m|e|V(x)]^{1/2}}, \tag{32}$$

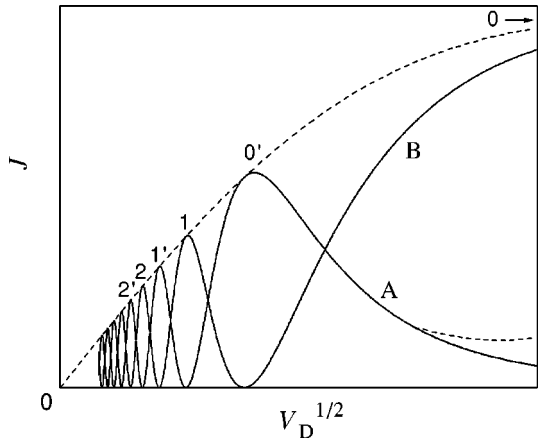

FIG. 5. A plot of the JV_D-characteristics for the ROS (A) and the RCS (B).

that is

$$2\int_0^l \delta k(x)dx=\left(\frac{2m}{|e|}\right)^{1/2}\left(\frac{\delta\epsilon}{\hbar}\right)\int_0^l\frac{dx}{\sqrt{V(x)}}.$$

The minimums of the current for the RCS coincide with the maximums for the ROS and vice versa. If the voltage drop across the DQWS is small, we can approximately write:

$$V_D^{(\pm)}(s)=\frac{2m}{|e|}\left(\frac{l\delta\epsilon}{\pi\hbar(2s+1/2\pm 1/2)}\right)^2. \tag{33}$$

A qualitative picture of the JV-characteristics is shown in Fig. 5. We note that the RCS JV-characteristic for high voltages, $V_D\to\infty$, tends asymptotically to the JV-characteristic of the ballistic diode without the DQWS[31] while the ROS tends to be locked. Actually this locking can be eliminated by nonresonant tunneling and nonballistic transport at high voltages.

Numerical results demonstrated below relate to the GaAs-QWs ($m=0{,}067m_o$, m_o is a free electron mass). The other parameters are: $L=l_1+l+l_2=0.5$ μm, $a=0.5$ μm, $N_b=5\cdot10^9\div5\cdot10^{10}\mathrm{cm}^{-2}$, $\delta\epsilon=1.5\div2.5$ meV, $\mu=1\div3$ meV, $T=4.2$ K, and $\epsilon_d=12.92$. We consider model samples with the centrally positioned DQWS and with the DQWS shifted to the anode. The energy of the longitudinal optical phonon in GaAs is $\hbar\omega_o=36$ meV. This value determines the highest reasonable voltages, $V_D\leqslant\hbar\omega_o/|e|$, when the ballistic electron transport holds. We suppose that the ballistic length is greater than 0.5 μm which does not contradict to the known experimental data (see, e.g., Refs. 4 and 15).

The calculated JV-characteristics are very similar to the curves shown in Fig. 5. Unfortunately we cannot obtain a stable numerical solution for low voltages. An interesting peculiarity of the calculated curves is a hysteresis of the transition between the high-current (HC) and low-current (LC) regimes which is a result of the Z-shape of the JV-characteristic. This means that in a certain voltage range there are several values of current (at least, three) for a given voltage V_D. The intermediate values of the current are not obtained since our calculations are performed for the given voltages V_D, and they give only the stable HC and LC solutions.

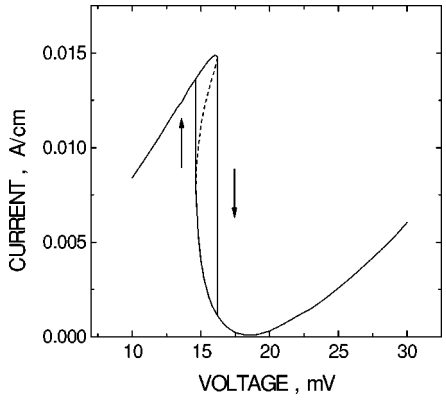

FIG. 6. An example of the Z-shaped dependence $J=J(V_D)$ for the ROS with parameters $\delta\epsilon=2.5$ meV, $\mu=3$ meV, $N_b=5\cdot10^9$ cm^{-2}, $l_1=l_2=0.15$ μm, $l=0.2$ μm.

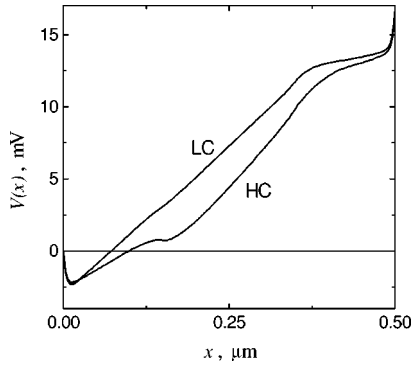

FIG. 8. Potential distributions $V(x)$ in the current conducting channel for the same diode as in Fig. 7.

An example of the JV-characteristic with the hysteresis for the ROS is demonstrated in Fig. 6. For this structure $l_1=l_2=0.15$ μm, $l=0.2$ μm, $\mu=3$ meV, $\delta\epsilon=2.5$ meV, $N_b=5\cdot10^9$ cm^{-2}. Distributions of the electron concentration $N(x)$ (Fig. 7; here and further we shift again the origin of coordinates to the plate C, i.e., to the cathode) and potential $V(x)$ (Fig. 8) for these HC and LC branches differ significantly. The HC branch is characterized by the high electron concentration in the DQWS and a jump with doubling of the concentration at $x=l_1$. On the other hand the LC branch has twice as low concentration in the DQWS and has no a similar jump. This variance results in the substantial difference between the potential distributions for these branches. In the LC regime the voltage drops mainly across the cathode-adjacent SQWS, and an electric field has no peculiarity at the SQWS/DQWS boundary. At the same time, the HC potential distribution is characterized by the substantially smaller electric field in the cathode-adjacent SQWS. A region with a large field is shifted into the DQWS, and nearly all anode voltage drops across the DQWS. The most distinctive detail of this distribution is a zero field region near the SQWS/DQWS junction (see Fig. 8).

JV-characteristics of the ROS and the RCS with $l_1=0.1$ μm, $l=0.4$ μm, $l_2=0$, $\mu=1$ meV, $\delta\epsilon=1.5$ meV, $N_b=1\cdot10^{10}$ cm^{-2} are presented in Fig. 9. A current maximum for the RCS and a current minimum for the ROS (where the current is scarcely different from zero) at $V_D=20$ mV correspond to the number $s=1$ in Fig. 5. Both characteristics have the last extrema at $V_D\sim80$ mV which are not shown. The multivalued behavior induced by a spatial charge redistribution is not displayed for low numbers s. The hysteresis related to the Z-shape of the characteristic appears at $V_D=7\div7.5$ mV for the RCS and at $V_D\simeq4.5$ mV for the ROS. We cannot calculate the stable JV_D-dependence at $V_D<4$ mV.

The potential distributions $V(x)$ for the RCS in the voltage range between V_a and V_b (see Fig. 9) are shown in Fig. 10. The main feature of these distributions is a presence of the second potential barrier for electrons near the SQWS/DQWS boundary. It is similar to an additional virtual cathode, and we named it a pseudocathode. The height of the pseudocathode increases with V_D. It is clear that the ballistic consideration becomes invalid for these voltages because of the existence of the new potential well between the effective cathode and the pseudocathode. Any electron trapped in this well due to scattering or in a different way cannot leave it ballistically. It leads to the filling of this potential well by the electrons and to the reconstructing of the distribution $V(x)$. Since our numerical procedure does not take into account inelastic scattering which is necessary for the trap of electrons in the well and the escape of electrons from the well,

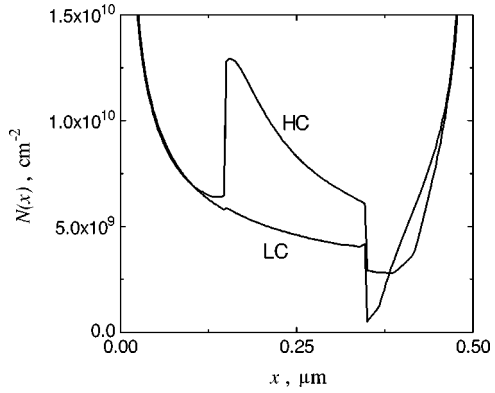

FIG. 7. Concentration distributions $N(x)$ in the diode with the ROS from Fig. 6 for the both current branches (HC is a high current branch, LC is a low current branch) at $V_D=15.5$ mV.

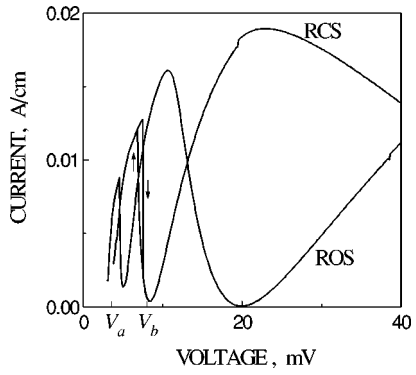

FIG. 9. JV_D-characteristics of the diodes with the ROS (A) and the RCS (B) with the same parameters: $l_1=0.1$ μm, $l=0.4$ μm, $l_2=0$, $\delta\epsilon=1.5$ meV, $\mu=1$ meV, $N_b=1\cdot10^{10}$ cm^{-2}.

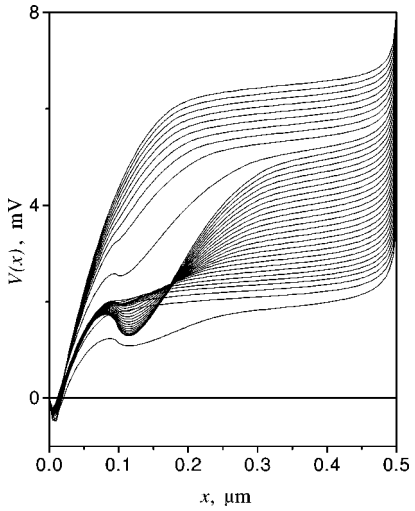

FIG. 10. Potential distributions $V(x)$ in the diode with the RCS from Fig. 9 for the successive voltages from V_a to V_b.

the numerical solution of the self-consistent ballistic problem is not adequate. Frequently under these conditions the calculation procedure becomes unstable.

At low voltages there exists another difficulty for the calculations dealing with the small distance between the rising branches for large s [see Eq. (33)]. It leads to multivalued behavior with more than three solutions for a given V_D. Transitions between these solutions become complicated.

The results presented in Figs. 6, 7, and 8 relate to the symmetrical structure with the equal anode- and cathode-adjacent SQWSs ($l_1=l_2$), while other results (Figs. 9 and 10) correspond to the bases without the cathode-adjacent SQWS ($l_2=0$). There are no principle advantages of one structure over another. Therefore, the design of the diode can be determined in accordance with technological preferences. In contrast to the cathode-adjacent SQWS, the anode-adjacent SQWS is set by the necessity to accelerate the electrons up to the single-velocity regime. If the acceleration is insufficient, the current modulation is incomplete (see Fig. 9).

From the technological point of view the RCS looks much simpler than the ROS, since the implementation of the RCS does not require back gates. The advantage of the ROS

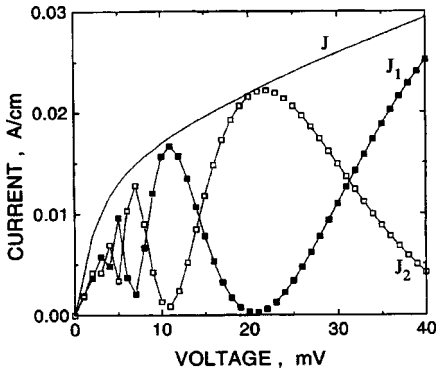

FIG. 11. JV_D- and $J_{1,2}V_D$-characteristics of the diode with the coupler structure; $\delta\epsilon=2$ meV, $\mu=3$ meV, $l_1=0.1$ μm, $l=0.4$ μm, $N_b=5\cdot10^9$ cm^{-2}.

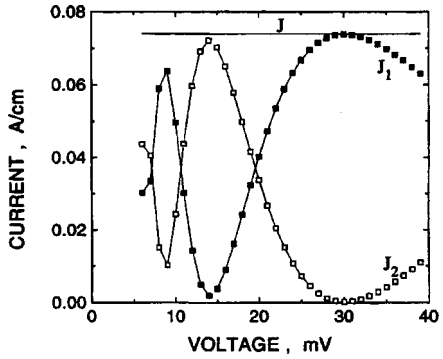

FIG. 12. JV_D- and $J_{1,2}V_D$-characteristics of the diode with the coupler structure; $N_b=5\cdot10^{10}$ cm^{-2}; the other parameters are the same as in Fig. 11.

is in an extended region with the N-type negative differential resistance (N-NDR) at high voltages. Of course, this advantage may be illusory because at high voltages ballisticity is disappearing, and nonresonant components of the tunnel current are rising. In addition, detuning of the tunnel resonance due to the recharging of the QWs in the DQW may be too large.

IV. RESULTS FOR COUPLER-STRUCTURES

We assume that both QWs forming the DQWS are in contact with the same anode plate A [$l_2=0$, Fig. 1(c)]. We neglected the details of the anode design in our calculations supposing that it is suitable to measure separately the anode currents J_1 and J_2. The dependence of the total current, $J=J_1+J_2$, as a function of V_D is monotonous and quite routine, while the partial currents $J_{1,2}$ oscillate in the range between zero and J:

$$J_1=J(V_D)t_b,\quad J_2=J(V_D)t_t. \tag{34}$$

The calculated results for coupler structures with $l_1=0.1$ μm, $l=0.4$ μm, $\mu=3$ meV, $\delta\epsilon=2$ meV are shown in Figs. 11 and 12 for two different values of N_b, $N_b=5\cdot10^9$ cm^{-2} and $5\cdot10^{10}$cm^{-2}, respectively. The current modulation is incomplete at low voltages V_D because a single-velocity regime is not realized. The total current in the lightly doped structure, $N_b=5\cdot10^9$ cm^{-2}, rises with the voltage (Fig. 11), and therefore the maximum values of the currents $J_{1,2}$ increase too. To provide the true coupler regime when the current is switched from one channel to the other without changing its value, we should increase the donor concentration N_b up to $5\cdot10^{10}$ cm^{-2}. As a result, the diode is in a saturation regime with $J=$const and the currents $J_{1,2}$ are practically equal to each other in their maximums (Fig. 12).

In reality, it is very difficult to implement the coupler structure because we have to independently contact with two closely spaced QWs on one side of the DQWS, and the anodes $A_{1,2}$ should be placed almost in the same point. Numerous methods described in Refs. 1–16 and other analogous works do not reach this goal, so new suggestions are needed.

V. DISCUSSION

First, we should note that the considered here design of the ballistic diode shown in Fig. 4 differs from the designs of

the structures with independent contacts described in Refs. 1–16. We assume that our results do not depend critically on geometry of the contacts. The assumption relates especially to the stationary characteristics considered here. Therefore, in the further discussion concerning the applicability of our results we have in mind not only our specific design (Fig. 4) but more universal designs as well.

Our calculations (Sec. III) show that the self-consistent potential under definite conditions may have the potential well between the effective and pseudocathode near the DQWS boundary. Therefore, the condition of the ballistic transport is not satisfied. A presence of the potential well sometimes leads to instability of the calculation scheme because electrons occasionally trapped in the well cannot leave it. As a result, they increase the spatial charge. This well occurs in the rising branches of the *JV*-characteristics near the current maxima at low voltages. At the same time the well is absent near the current minima, and near the high-voltage maxima where there are only inflection points as certain rudiments. This means that the high-voltage region and the descending branches at low voltages are reliable. Consequently, the *JV*-characteristics with N-NDR having an extremely low valley currents take place certainly. The positions of the current maxima at low voltages and especially the high-current branch of the Z-shaped sections (i.e., the boundaries of the hysteresis regions) are unreliable.

The situation with the potential well in front of the DQWS reminds us of the situation with an accumulation layer in front of a two-barrier structure of a resonant tunneling diode.[32] The existence of such a layer requires us to take into account inelastic scattering mechanisms in order to calculate correctly a self-consistent potential and electron concentration. This problem is not solved here.

Among other simplifications, the symmetry of the wells, which is necessary for a sharp tunnel resonance has been assumed. A precision of the resonance tuning, that is the difference of individual quantization energies has to be within SAS-splitting (i.e., $\sim 2 \div 3$ meV). A detuning decreases the current modulation level substantially. (Such a decrease considered in Refs. 23 and 26 for a linear conductance of the ROS/RCS.) Since the top- and the bottom-wells are different initially (see, e.g., Refs. 5, 6, and 33), an additional well symmetrization has to be provided. A back gate with a large enough area under a substrate could be convenient for this goal. The applied voltages V_D should not induce a large detuning of the tunnel resonance, so we have

$$|eV_D| \ll \delta\epsilon C/C_g, \tag{35}$$

where C is an interwell capacity, C_g is a capacity of the DQWS and the back gate above mentioned.

In addition to the resonance detuning considered above there exists one more detuning mechanism dealing with the tunnel electron transfer itself. This mechanism which is responsible for the considering effects, can affect the transfer appreciably since it impedes a full tunnel resettlement. This impediment is small if a condition

$$Ae^2N \ll 2C\delta\epsilon \tag{36}$$

is satisfied, where A is a DQWS area, and N is a sheet electron concentration ($[\mathrm{cm}^{-2}]$). If $C/A=\epsilon_d/d$, where d is an effective distance between charge centers in the wells, Eq. (36) can be rewritten in the form

$$N \ll 2\epsilon_b \delta\epsilon/e^2 d. \tag{37}$$

We obtain on the right-hand side of Eq. (37) a concentration $\sim 3\cdot 10^{10}$ cm^{-2} for $\delta\epsilon=2$ meV and $d=10^{-6}$ cm. We can satisfy the condition (36) by increasing $\delta\epsilon$ and decreasing d (they do not contradict each other).

Since we have accepted the condition of the classic (i.e., multimode) electron transport in the resonant DQWS, we are limited in the increase of $\delta\epsilon$. This additional condition is unnecessary but convenient when the interwell tunnel current oscillations, the CO-1, (Sec. III), are considering only, while the resonant quantum current oscillations, the CO-2, prove to be suppressed. The CO-2 are determined by the eigenvalues of an electron cavity in the DQWS and are enveloped by the CO-1 due to their smaller period. A condition of the suppression of the CO-2 and justification of the classic approach is

$$\Delta\lambda \gg \lambda/r \simeq \lambda^2/l, \tag{38}$$

where $\lambda=\lambda_{\mathrm{DQW}}$ is a mean electron wave length in the DQWS [see Eq. (1)], $r\simeq l/\lambda \gg 1$ is a number of the resonator mode, and $\Delta\lambda$ is a dispersion of λ. The dispersion of the energy $\epsilon \simeq \epsilon_x$ is estimated by the energy width of the entering electron beam

$$\Delta\epsilon = \frac{h^2\Delta\lambda}{m\lambda^3} \simeq \mu - |eV_m| \equiv \mu^*. \tag{39}$$

Then condition (38) transforms into the form

$$\mu^* \gg h v_{\mathrm{DQW}}/l. \tag{40}$$

In accordance with Eqs. (31) and (32) we can approximately write $v_{\mathrm{DQW}} \simeq l\delta\epsilon/\pi\hbar s'$, where $s'=s+1/4\pm 1/4$ and we have

$$\mu^* \gg 2\delta\epsilon/s'. \tag{41}$$

A condition of a single–velocity regime which has to be satisfied together with Eq. (41) is

$$\mu^* \ll 2\epsilon_x/s' \simeq 2|eV_D|/s'. \tag{42}$$

An insufficient satisfaction of Eq. (42) for low voltages and large values of s' makes the current modulation level lower.

Merging all the energy inequalities [Eqs. (37), (41), and (42)] we have the hierarchy

$$e^2Nd/2\epsilon_b \ll \delta\epsilon \ll s'\mu^*/2 \ll |e|V_D < \hbar\omega_o. \tag{43}$$

All these inequalities excluding Eq. (41) have been satisfied in our calculations. We carried out a series of additional calculations with large values of μ (up to 6 meV) and high donor concentrations (up to $5\cdot 10^{10}$cm^{-2}) to raise μ^*. These increases in μ and N_b raise the maximum current substantially but do not change qualitative behavior of JV_D-dependences for high voltages V_D (>15 mV). At the same time the current oscillations for low voltages (<15 mV) are resolved less clearly because the single-velocity re-

gime is nearly washed out in agreement with the condition (42). Therefore we have presented in Sec. III the results for smaller values of μ and N_b.

A suppression of the CO-2 can also occur due to fluctuations of the DQWS length l with a dispersion

$$\delta l \geqslant \lambda \simeq l/r. \tag{44}$$

If $l=0.3$ μm and $r=10$ (it is a realistic number), $\delta l=30$ nm is sufficient to suppress the CO-2 completely.

In the Appendix we present a set of accurate formulae for the coefficients of transmission in the model ROS and RCS without taking into account a spatial charge (in linear approximation). These formulae show the character of the influence of the CO-2 clearly. Since the CO-2 can be obtained as a result of the quasiclassical quantization of longitudinal electron motion in the DQWS, they can be considered precisely in the frameworks of our procedure but with substantial variations. We have to calculate and to remember full electron phases in both QWs instead of only the phase difference $\xi(x)$. It is a much more cumbersome problem.

VI. CONCLUSIONS

We enumerate the main results obtained above.

(1) The resonant DQWSs embedded into the base of the ballistic diode (the ROS or the RCS) lead to multimaximum and multiminimum JV-characteristics (the CO-1) with repeated falling branches and N-NDR (Fig. 5). The ROS (the ballistic Eisenstein-type structure) which is more complicated technologically than the RCS has no principle advantages in comparison with the RCS (excepting an asymptotic behavior for high voltages).

(2) At low voltages these characteristics can demonstrate multivalued current behavior and Z-shaped sections. The number of the current extrema depends on the energy width μ^* of the electron beam in the DQWS.

(3) There is another type of multimaximum behavior of the JV-characteristics named the CO-2. It is not discussed thoroughly here. The oscillations can complicate the described picture if they are not suppressed. The suppression occurs for large values of μ^* and/or for noticeable inhomogeneous fluctuations of the DQWS length l. A classical approach developed and used above is justified in these cases.

(4) A nonresonant coupler-structure displays multiextremum behavior for the partial currents $J_{1,2}$, but does not demonstrate such behavior for the total current J. The oscillations of the partial currents corresponds to the switching of the current J between the anodes A_1 and A_2. The switching can be controlled both by the voltage V_D using the peculiarities of the $J_{1,2}V_D$-characteristics considered above and by a potential of an additional gate varying a SAS-splitting $\delta\epsilon$ and an electron concentration N, as is usually done. Nevertheless, we have to note that technological problems of independent contacts to the wells forming the DQWS for the coupler-structure have no successful solution up at the present time.

With increasing the electron concentration N effects of Coulomb interactions between electrons from the different QWs can create substantial corrections in the considered solutions. These effects have not been taken into account here.

We hope that the presented here results will initiate an interest of experimentalists to fabricate shorter than in[1–16] ballistic overlap structures, as well as to the cover structures, which have not implemented yet.

ACKNOWLEDGMENTS

The authors thank N. Z. Vagidov, B. Glavin, and O. Melnikova for their friendly help. We would like to acknowledge gratefully the support from the NSF and the ARO.

APPENDIX: TRANSMISSION IN A LINEAR APPROXIMATION

Formulas for transmission coefficients of linear homogeneous resonant overlap and cover structures are collected in this Appendix. We have for the ROS:

$$T=\frac{64k'k''}{|D|^2}\chi_1^2\chi_2^2(\chi_1-\chi_2)^2(k_2\ \sin\ k_1l-k_1\ \sin\ k_2l)^2, \tag{A1}$$

where

$$\begin{aligned}D=&2\cos\psi[(\chi_1^2+\chi_2^2)(k'k''+k_1k_2)\\&-\chi_1\chi_2(k_1^2+2k'k''+k_2^2)]-2\cos 2\delta[(\chi_1^2+\chi_2^2)\\&\times(k'k''-k_1k_2)-\chi_1\chi_2(k_1^2+2k'k''+k_2^2)]-8k_1k_2\chi_1\chi_2\\&-2i\ \sin\ \psi[\chi_1^2(k'k_1+k''k_2)+\chi_2^2(k'k_2+k''k_1)\\&-\chi_1\chi_2(k'+k'')(k_1+k_2)]-2i\ \sin 2\delta[\chi_1^2(k''k_2-k'k_1)\\&+\chi_2^2(k'k_2-k''k_1)+\chi_1\chi_2(k'+k'')(k_1-k_2)],\end{aligned}$$

$$\chi_{1,2}=-\frac{1}{2\delta\epsilon}[\epsilon'-\epsilon''\pm\sqrt{(\epsilon'-\epsilon'')^2+4(\delta\epsilon)^2}],$$

$\psi=(k_1+k_2)l$, $\delta=1/2(k_1-k_2)l$ is similar to $\xi(l)$ in Sec. II, ϵ' and ϵ'' are the ground levels of quantization in the isolated bottom- and top-wells, k' and k'' are x-components of wave vectors in the bottom and top-wells outside the DQWS for a given energy, k_1 and k_2 are the same components of the SAS-splitted waves inside the DQWS for the same energy.

Equation (A1) is simplified for sharp tuning of the tunnel resonance when $\chi_1^2=\chi_2^2=1$, $\chi_1\chi_2=-1$. For the energy of electrons much greater than $\delta\epsilon$ we have

$$k_1\simeq k_2\simeq k'\simeq k''=k, \tag{A2}$$

$$T=\frac{2\sin^2\ \delta(1+\cos\ \psi)}{1+\sin^4\ \delta+2\sin^2\ \delta\cos\ \psi}. \tag{A3}$$

Both a phase δ which is responsible for the CO-1 and a phase ψ which is responsible for the CO-2 are presented in Eq. (A3) as well as in initial Eq. (A1). To exclude the phase ψ we have to average T on a period:

$$\langle T\rangle=\frac{1}{\pi}\int_{n\pi}^{(n+1)\pi}T(\psi)d\psi. \tag{A4}$$

Using Eqs. (A3) and (A4) we obtain

$$\langle T\rangle = \frac{2\sin^2\delta}{1+\sin^2\delta}, \tag{A5}$$

as in Eq. (22) for the nonlinear case.

For the RCS we have

$$\begin{aligned} T = {} & \frac{32(k')^2}{|D|^2}(\chi_1-\chi_2)^2[(1-\cos\psi\cdot\cos 2\delta) \\ & \times(\chi_1^2k_2^2+\chi_2^2k_1^2)-2k_1k_2\chi_1\chi_2(\cos 2\delta-\cos\psi) \\ & +\sin\psi\cdot\sin 2\delta\cdot(\chi_1^2k_2^2-\chi_2^2k_1^2)], \end{aligned} \tag{A6}$$

where

$$\begin{aligned} D = {} & 2\cos 2\delta\{\chi_1^2[(k')^2+k_2^2]+\chi_2^2[(k')^2+k_1^2] \\ & +2\chi_1\chi_2[(k')^2-k_1k_2]\} \\ & -2\cos\psi\{\chi_1^2[(k')^2+k_2^2]+\chi_2^2[(k')^2+k_1^2] \\ & -2\chi_1\chi_2[(k')^2+k_1k_2]\} \\ & -8\chi_1\chi_2(k')^2+4ik'(\chi_1-\chi_2)[(\chi_1k_2+\chi_2k_1) \\ & \times\sin 2\delta+(\chi_1k_2-\chi_2k_1)\sin\psi], \end{aligned}$$

and instead of Eq. (A3)

$$T = \frac{2\cos^2\delta(1-\cos\psi)}{1+\cos^4\delta-2\cos^2\delta\cos\psi}. \tag{A7}$$

Equation (A4) gives for this case

$$\langle T\rangle = \frac{2\cos^2\delta}{1+\cos^2\delta}, \tag{A8}$$

and it is similar to Eq. (26).

[1] J. Smoliner, W. Demmerle, G. Berthold, E. Gornik, and G. Weimann, Phys. Rev. Lett. **63**, 2116 (1989).
[2] W. Demmerle, J. Smoliner, G. Berthold, E. Gornik, G. Weimann, and W. Schlapp, Phys. Rev. B **44**, 3090 (1991).
[3] J. P. Eisenstein, L. N. Pfeiffer, and K. W. West, Appl. Phys. Lett. **57**, 2324 (1990).
[4] J. P. Eisenstein, Superlattices Microstruct. **12**, 107 (1992).
[5] N. K. Patel, J. H. Burroughs, M. J. Tribble, E. H. Linfield, A. C. Churchill, D. A. Ritchie, and G. A. C. Jones, Appl. Phys. Lett. **65**, 851 (1995).
[6] N. K. Patel, M. P. Grimshaw, J. H. Burroughs, M. L. Leadbeater, D. A. Ritchie, and G. A. C. Jones, Appl. Phys. Lett. **66**, 848 (1995).
[7] K. M. Brown, E. H. Linfield, D. A. Ritchie, G. A. C. Jones, M. P. Grimshaw, and A. C. Churchill, J. Vac. Sci. Technol. B **12**, 1293 (1994).
[8] E. H. Linfield, G. A. C. Jones, D. A. Ritchie, and J. H. Thompson, Semicond. Sci. Technol. **8**, 415 (1993).
[9] J. P. Eisenstein, L. N. Pfeiffer, and K. W. West, Appl. Phys. Lett. **58**, 1497 (1991).
[10] K. M. Brown, E. H. Linfield, D. A. Ritchie, G. A. C. Jones, M. P. Grimshaw, and M. Pepper, Appl. Phys. Lett. **64**, 1827 (1994).
[11] J. P. Eisenstein, L. N. Pfeiffer, K. W. West, Phys. Rev. Lett. **69**, 3804 (1992).
[12] K. M. Brown, N. Turner, J. T. Nicholls, E. H. Linfield, M. Pepper, D. A. Ritchie, and G. A. C. Jones, Phys. Rev. B **50**, 15 465 (1994).
[13] N. Turner, J. T. Nicholls, E. H. Linfield, K. M. Brown, G. A. C. Jones, and D. A. Ritchie, Phys. Rev. B **54**, 10 614 (1996).
[14] J. P. Eisenstein, L. N. Pfeiffer, K. W. West, Phys. Rev. Lett. **68**, 674 (1992).
[15] I. S. Millard, N. K. Patel, M. Y. Simmons, E. H. Linfield, D. A. Ritchie, G. A. C. Jones, and M. Pepper, Appl. Phys. Lett. **68**, 3323 (1996).
[16] J. P. Eisenstein, T. J. Gramila, L. N. Pfeiffer, and K. W. West, Phys. Rev. B **44**, 6511 (1991).
[17] J. A. del Alamo and C. C. Eugster, Appl. Phys. Lett. **56**, 78 (1990).
[18] N. Tsukada, A. D. Wieck, and K. Ploog, Appl. Phys. Lett. **56**, 2527 (1990).
[19] C. C. Eugster, J. A. del Alamo, M. J. Rooks, and M. R. Melloch, Appl. Phys. Lett. **64**, 3157 (1994).
[20] Y. Hirayama, Y. Tokura, A. D. Wieck, S. Koch, R. J. Haug, K. von Klitzing, and K. Ploog, Phys. Rev. B **48**, 7991 (1993).
[21] R. Q. Yang and J. M. Xu, Phys. Rev. B **43**, 1699 (1991).
[22] J. Q. Wang, S. Q. Yuan, B.-Y. Gu, and G. Z. Yang, Phys. Rev. B **44**, 13 618 (1991).
[23] Z. S. Gribnikov, Fiz. Tekh. Poluprovodn. **26**, 996 (1992).
[24] Z. S. Gribnikov, Zh. Eksp. Teor. Fiz. **103**, 1329 (1993); JETP **76**, 651 (1993).
[25] J. Q. Wang and B.-Y. Gu, Phys. Rev. B **47**, 13 422 (1993).
[26] N. Z. Vagidov and Z. S. Gribnikov, Fiz. Tekh. Poluprovodn. **26**, 2068 (1992).
[27] N. Z. Vagidov and Z. S. Gribnikov, Lith. Phys. J. **32**, 61 (1992).
[28] Z. S. Gribnikov, A. N. Korshak, S. I. Kozlovsky, and N. Z. Vagidov, Lith. Phys. J. **36**, 599 (1996).
[29] N. Z. Vagidov, Z. S. Gribnikov, and A. N. Korshak, Semiconductors **28**, 1033 (1994); **29**, 286 (1995); **29**, 1014 (1995).
[30] Z. S. Gribnikov, A. N. Korshak, N. Z. Vagidov, and Z. M. Alexeeva, in *Proceedings of the 23rd International Conference on Physics of Semiconductors* (World Scientific, Singapore, 1996), Vol. 4, p. 3287.
[31] N. Z. Vagidov, Z. S. Gribnikov, and A. N. Korshak, Semiconductors **29**, 286 (1995).
[32] E. R. Brown, in *Heterostructures and Quantum Devices*, edited by N. G. Einspruch and W. R. Frensley (Academic, San Diego, CA, 1994), p. 306.
[33] B. Kardynal, E. H. Linfield, D. A. Ritchie, K. M. Brown, C. H. W. Barnes, G. A. C. Jones, and M. Pepper, Appl. Phys. Lett. **68**, 826 (1996).